Capabilities and performance of the CLEAR facility photo-injector laser

E. Granados, E. Chevallay, V. Fedosseev, and H. Panuganti
CERN, EN department, CH-1211, Geneva (Switzerland)

Abstract
This paper describes the current functionality and newly implemented capabilities of the CLEAR facility photo-injector laser. The primary focus for CLEAR is general R&D and component studies for existing and future machines at CERN. Accordingly, its photo-injector laser system has been upgraded in order to accommodate for a large range of experimental setups and tests. The systems and performance presented here have been developed with a view on improving the CLEAR injector flexibility, reliability and its systematic optimization.

Keywords
CLEAR; photo-injector; UV laser; RF-gun.

CERN-OPEN-2020-002
01/09/2019

1 Introduction

The aim of the present report is to present the modifications and performance of the CLEAR photo-injector laser after the upgrades carried out during 2018/2019. These improvements were implemented in order to fulfill the requirements of the CLEAR program, with experimental tests planned for the period 2018-2022.

CLEAR arises from the experience acquired during the CLIC test facility 3 (CTF3). Before shut-down at the end of 2016, CTF3 demonstrated the feasibility of the CLIC key concepts. The CTF3 developments made available key expertise, space and equipment, which triggered the interest of a broad community within and outside CERN for accelerator R&D. A proposal to adapt and reuse a large part of the CTF3 facility was submitted to the CERN management, which supported the project for an initial period of 2+2 years, with a review between the two terms [1].

The resulting "CERN Linear Electron Accelerator for research" (CLEAR) is a new stand-alone user facility, with the following goals: Accelerator R&D, support of high-gradient acceleration concepts, create a test-bench for beam instrumentation, boost collaboration with other science fields (such as X-ray FELs, medical, space and industrial communities), and maintain training capabilities for the next generation of accelerator scientists and engineers.

Within CTF3, CALIFES (Concept d'Accelerateur Lineaire pour Faisceau d'Electron Sonde) is an electron linac which provided a flexible electron beam for tests built in collaboration among LAL, RAL and CERN [3, 4, 6]. The CLEAR photo-injector is based on the CALIFES RF-gun, and even though it may not be optimal for the CLEAR experimental program, its location, performance, and existing infrastructure make the CALIFES RF-gun a cost-efficient solution for the CLEAR experimental purposes.

The CALIFES RF-gun was constructed with the following parameters:

- Charge of 1.5 GHz electron micro bunch: 0.6 nC;
- Macro bunch length: 150 ns;
- Current within the macro bunch: 0.93 A (for a train of 32 bunches);
- Normalized emittance: < 20 π-mm-mrad (for high charge mode, 0.6 nC/bunch);
- Photo-cathode quantum efficiency: QE > 0.3 % (over > 200 hours, initial QE $\sim 3\%$);
- UV laser pulses energy: > 370 nJ;
- Charge stability: $< 3\%$ rms.

2 Laser system

In this section, the main components of the CLEAR photo-injector laser system are described. The current optical chain of the laser is the result of several modifications during the lifetime of the CTF3 facility. Consequently, the aim of this description is to give a comprehensive view of the current state of the laser system and overall performance.

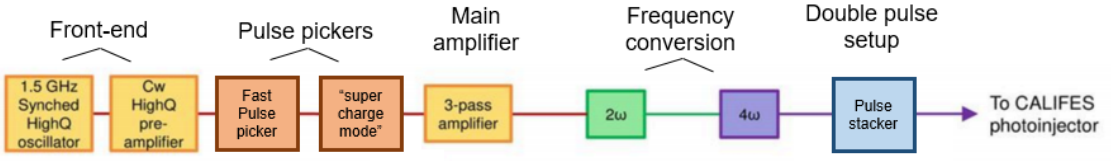

Figure 1: Simplified schematic of the CLEAR laser setup.

The production of electron bunches in the RF-gun is based on Cs_2Te photo-cathode technology, which generally requires low UV power illumination for operating efficiently [5]. Lifetime of the photo-cathode is one of the main concerns due to the vacuum level in the RF gun. Consequently, the CLEAR RF-gun is equipped with photo-cathode regeneration in-situ by utilizing built-in Cs evaporators. This allows fast recovery of the photo-cathode quantum efficiency on-demand.

The UV pulses with the required repetition rate and pulse energy are produced by a home-built all-solid-state Nd:YLF system [7]. This laser system is composed of oscillator and pre-amplifier, main amplifier and frequency quadrupling stage as depicted in Figure 1. The UV laser source is centered at 262 nm, with a laser pulse energy of >370 nJ/pulse (although laser energies of up to 1.5 μJ on the photo-cathode surface have been demonstrated).

The pulse energy was initially regulated by a hard aperture, producing a maximum bunch charge of up to 0.6 nC with a frequency of 1.5 GHz. This aperture was removed from the optical chain during the 2018 upgrades, mainly because the spot size is currently controlled by a variable magnification telescope. This modification allowed to generate up to 1.5 nC/bunch [1] when the spot size on the photo-cathode was magnified. Further foreseen developments include the commissioning of a remote controlled variable size aperture in order to enable the generation of variable size flat-top beams on the cathode with optimized fluence.

Trains ranging from 1 to 300 bunches have been tested successfully, although the current pulse picker system capability limits the pulse train duration to approximately 120 ns (180 bunches). An additional pulse picker system was installed during 2019 in order to increase the train length capability to 1500 bunches/train. The resulting laser performance parameters are summarized in Table 1.

Table 1: Current CLEAR photo-injector laser parameters.

Laser parameter	**Value range**
Energy onto the cathode [μJ/bunch]	Up to 1.5
Intensity stability rms	<1.5%
Spot diameter on the cathode σ [mm]	0.8-1.5
Pointing stability onto the cathode rms	<0.2
Wavelength [nm]	262
Micro-bunch length FWHM [ps]	4.7
Micro-bunching frequency [GHz]	1.5
Micro-bunch train length	1-180
Micro-bunch train length (supercharge mode)	1-1500
Repetition rate [Hz]	0.833 to 5

Other CLEAR laser upgrades included the implementation of a double pulse setup, new encoded motorization, digital diagnostic systems, and the refurbishment of the diode pumping system for the laser front-end. The upgrades produced excellent results in terms of intensity stability and available pulse energy, which is described in the following sections. Additionally, the aforementioned upgrades in combination with the refurbishment of the laser cooling systems have enabled the operation of the system 24/7, with brief shut-downs for maintenance and optimization (once per week).

2.1 Front-end

The front-end of the CLEAR photo-injector laser is composed of a Nd:YLF oscillator and pre-amplifier, with the specifications shown in Table 2. This laser has been used for multiple projects at CERN, including the PHIN photo-injector development [9].

Table 2: Front-end laser main performance parameters.

Laser parameter	Value range
Laser gain medium	Nd:YLF
Wavelength	1047 nm
Operation mode	CW mode-locked
Pulse repetition rate (locked)	1499.274956 MHz $\pm$ 2.3 Hz
Average power oscillator	0.3 W
Average power pre-amplifier	10.14 W
Pulse width	5.3 ps
Timing jitter	$<$0.3 ps rms
Beam quality	M^2 = 1.1
Beam pointing stability	σ = 25 μrad
Power stability (after warm-up time)	$<$0.56% over 13 h

2.1.1 Oscillator

The seed pulses are produced by a diode-pumped Nd:YLF mode-locked oscillator at a repetition rate of 1.5 GHz with an average power of $\sim$300 mW at 1047 nm. The output pulse duration is $\sim$ 5 ps. The pumping diode current is normally set to 1.5 A.

The synchronization with the RF reference is obtained at the laser oscillator level. The frequency (or repetition rate) of the oscillator is compared to the RF reference, and a PLL acts on the laser cavity end-mirror through a fast piezo-controller in order to stabilize it (with a feedback loop bandwidth of up to several 10 kHz). Because of the small tuning range of the laser oscillator, the cavity length needs to be initially adjusted manually to a value close to the RF reference in order to lock it (with a precision of the order of a few kHz). The base plate of the front-end laser is temperature stabilized by water cooling using a chiller with a temperature stability of 0.01K, ensuring stable operation of the locking system.

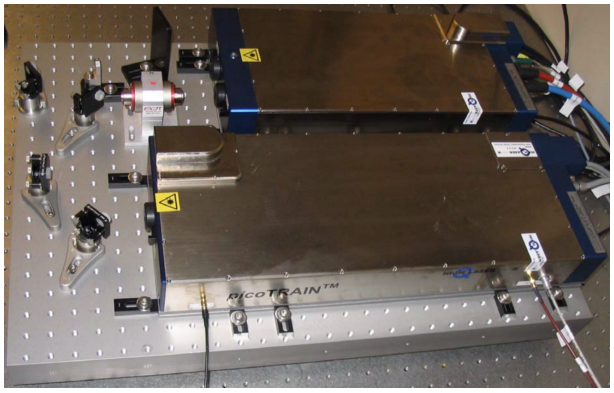

Figure 2: The picoTRAIN Nd:YLF oscillator (foreground), preamplifier and coupling optics

After initial commissioning, a time jitter of $<$100 fs rms has been measured [8] . However, during day to day operations, the estimated value for the time jitter is of the order of 300 fs rms. This value is a rough estimation based on the output from the laser's PLL, delivered by the laser control system.

The estimation of the timing jitter between the laser and the RF reference can be better approximated by measuring the phase noise spectrum of the output of the oscillator when is locked. Here, phase noise is defined as the one-sided spectral density of the signal phase deviation with respect to the RF

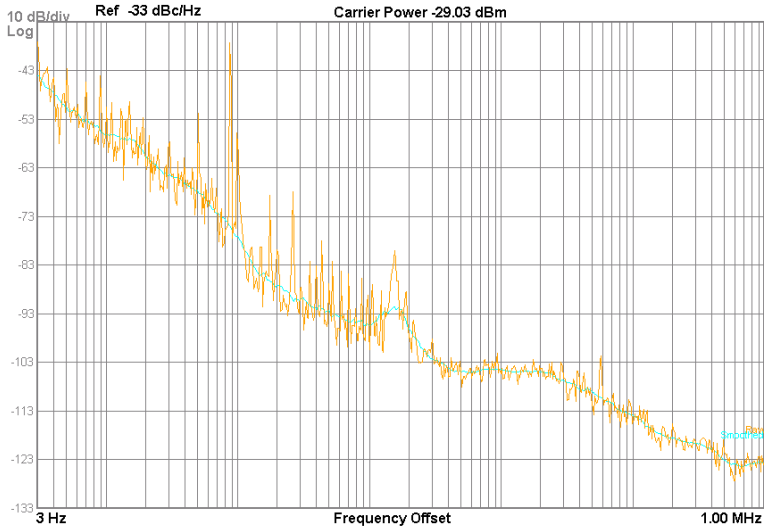

Figure 3: Trace of the phase noise measurement of the CLEAR laser output in closed loop (includes the phase noise of the RF reference).

carrier frequency.

The first step in calculating the equivalent rms jitter is to obtain the integrated phase noise power over the frequency range of interest. For laser oscillators, this range is usually given between 10 Hz and 1 MHz, although definitions vary. Since we are measuring the phase noise spectrum of the output of the laser, it already contains the phase jitter contribution of the RF reference. Therefore, the result of this estimation will be an upper limit for the timing jitter.

To perform the phase noise measurement we utilized a Keysight Technologies N9020A MXA Signal analyzer, with a frequency range from 10 Hz to 26.5 GHz. The maximum analysis bandwidth for the analyzer was 160 MHz, with a phase noise floor of -136 dBc/Hz at 1 MHz offset and -114 dBc/Hz from 3 Hz up to 30 kHz offsets. This yields an approximate instrumental rms timing jitter of < 100 fs.

Selecting the lower frequency for the integration requires some judgment. In theory, it should be as low as possible to get the true rms jitter [10]. In practice, however, the oscillator specifications are not generally given for offset frequencies smaller than 10 Hz. A lower frequency integration of 100 Hz is reasonable in most cases, and so both integration values are given here. For the case of the CLEAR front-end, given the fact that the locking system of the oscillator compensates fluctuations in the RF phase of > 10 kHz, we take into consideration a conservative integrated residual phase noise in the 1 kHz - 1 MHz band for calculating the rms phase jitter and the time jitter. This integration of the phase noise yields a value for the rms phase jitter of around 2.3 mrad, with a timing jitter < 250 fs, well below the specification of 1 ps.

Table 3: Estimation of rms timing and phase jitter for different phase noise integration frequency ranges.

Frequency Range	**rms Phase jitter (rads)**	**rms jitter (laser + RF)**
3 Hz - 1 MHz	0.0133	1.41 ps
10 Hz - 1 MHz	0.008	853 fs
100 Hz - 1 MHz	0.0028	293 fs
1 kHz - 1 MHz	**0.0023**	**247 fs**

The laser oscillator requires periodic intervention (about $\sim$ 1 per month) to ensure reliable long-term operation. Typically, the optimization involves the following steps:

- Maximizing the output power of the oscillator adjusting its cavity end-mirror.
- Adjusting the oscillator cavity length to matched it approximately to the RF reference frequency (1.499275 GHz $\pm$ 1 kHz) in open loop;
- Maximizing oscillator tuning range by ensuring that the piezo DC position is at the center of the tuning range when the oscillator is locked to the RF reference;
- Alignment of seed injection into the pre-amplifier;
- Maximize the output of the pre-amplifier by tuning the temperature of its diode stack cooling unit (described in the next section);

2.1.2 Pre-amplifier

The oscillator output pulses are firstly amplified by a Nd:YLF pre-amplifier in order to boost the available average power up to $\sim$ 10 W. The pulses delivered by the pre-amplifier have the same temporal characteristics (5.3 ps pulse duration at 1047 nm) as the oscillator pulses. The tuning of the wavelength of the pumping diodes of the pre-amplifier is performed by temperature adjustment of its chiller with 0.1K increments. This chiller actively stabilizes the temperature of the pumping diode stack enclosure. As the diodes degrade with use, it is required to adjust the temperature set point (usually by lowering it), in order to match the emission wavelength of the diode stack to the peak of the absorption cross-section spectrum of Nd:YLF.

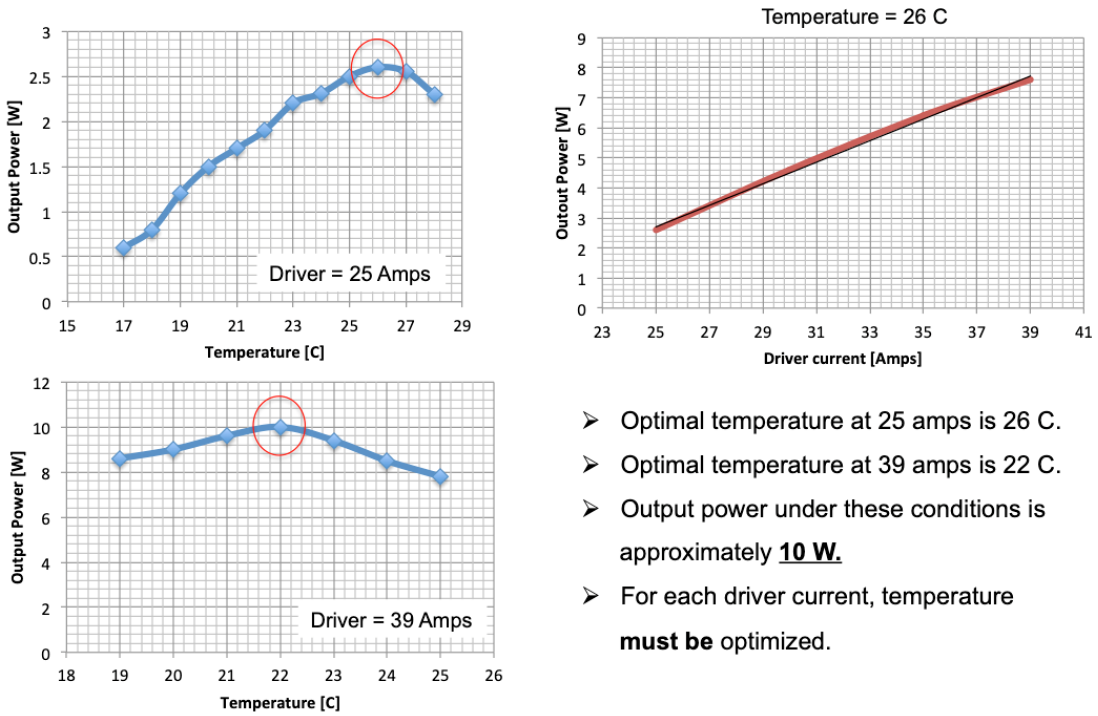

Figure 4: Optimization of the output power of the front-end by tuning the diode temperature of the pre-amplifier at different current settings.

It is important to note that the optimal temperature for the diode stack is dependant on its current setting. In order to achieve 10 W average power operation, it is required to set the current to ap-

proximately 39 A. Figure 4 shows examples of tuning curves with different driver currents and chiller temperatures.

The overall stability of the photo-injector laser relies heavily on the stability of the front-end laser. Accordingly, its output power has been measured continuously for periods of 8 hours. Nominally, the output power is 10.14 W, although in order to extend the lifetime of the pumping diodes, the current of the pre-amplifier has been set to 37 A, producing around 7 W of output power. This is enough power for saturated amplification in the main amplifier and efficient frequency conversion to the UV. Figure 5 shows the output average power stability of the front-end laser. As it can be seen, the average power is 10.14 W while the stability is approximately 0.3% rms with peak to peak variations of up to 2.15%.

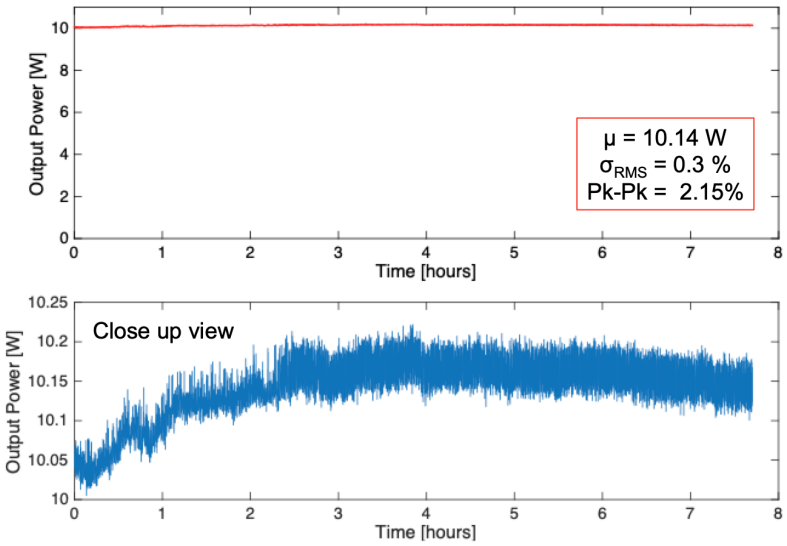

Figure 5: Output average power of the laser pre-amplifier measured during 8 hours.

2.2 Pulse picker systems

The pulse picking system of the CLEAR laser is composed by three different pulse picking systems as depicted in Figure 6.

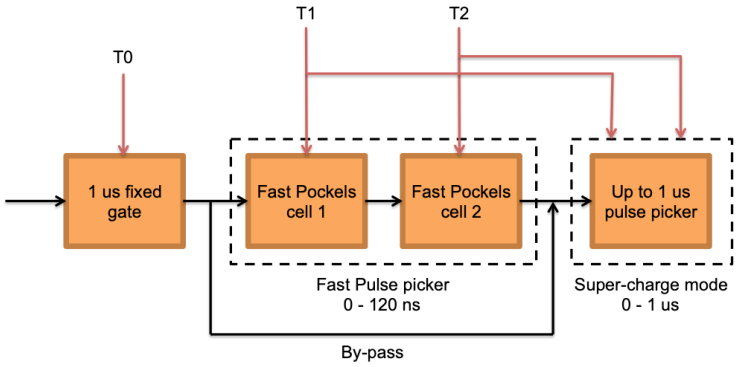

Figure 6: CLEAR pulse picker system schematic.

The first one, a commercial pulse picker from Leysop, consists in a fixed width window with

duration of 1 μs, which main purpose is to limit the input average power into the main amplifier. This pulse picker is triggered by a delay generator controlled from the CLEAR laser lab, although externally triggered by the CLEAR facility timing system.

The second pulse picker, commonly known as 'fast pulse picker', was constructed by CEA and designed for allowing discrimination of single pulses from the laser front-end at 1.5 GHz repetition rate (achieved with a pulse picker with rise-time < 400 ps). A third pulse picker (super-charge mode) has been placed at the output of the fast pulse picker to enable the production of longer pulse trains of up to 1 μs. Note that the fast pulse picker and the super-charge mode pulse picker do not operate simultaneously.

2.2.1 Fast pulse picker

The fast pulse picker is composed by 2 Pockels Cells and 3 polarizers as depicted in Figure 7. Dry KD*P cells where selected in order to avoid degradation of commonly used fluid filled Pockels cells on a long term scale. As it is shown, the input polarization into the first polarizing beam splitter (P1) is vertical. This polarizer defines the input polarization into the fast pulse picker. The polarization is then rotated by 90 degrees when PC1 is triggered. Under this configuration, all the pulses propagating through PC1 are normally reflected by P2, except during the time that the voltage is applied to PC1, being transmitted by P2. Since the pulse duration of the voltage signal applied to PC1 is fixed (120 ns duration), the number of pulses transmitted through P2 remains constant (180 laser pulses).

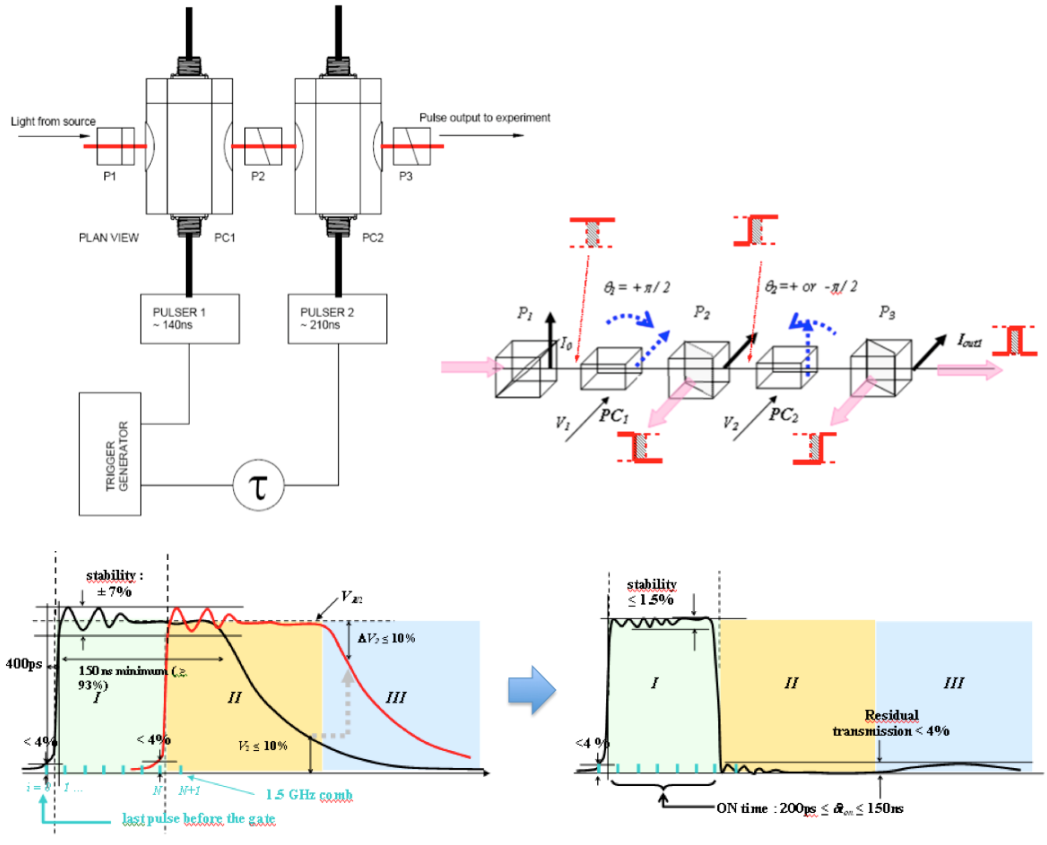

Figure 7: Fast pulse picker schematic (top left) and principle of operation (top right). Specifications of the time profile of the fast pulse picker. (bottom left) Individual profiles of PC1 and PC2. (bottom right) Expected performance after amplification. (Extracted from [2]).

The PC2 timing defines the closure of the time window for the pulse picker. When the transmitted

pulses via P2 impinge PC2, their polarization is again turned by 90 degrees while the voltage applied to PC2. Analogously to P2, P3 selects the horizontally polarized portion of the incoming pulse train.

PC1 and PC2 are driven by a high voltage pulse generator (from FID technologies). The pulse generators are triggered externally by a low timing jitter (< 30 ps) trigger from the CLEAR facility.

The main specifications for the fast pulse picker include a sharp rise time of less than 400 ps, with an amplitude stability or modulation within the transmission window of <1%. In the commissioning experiments in 2008, a rise time of 260 ps in the electrical signal was measured, whereas the optical signal showed a rise time of 350 ps. In terms of residual transmission, it was estimated to be <4% for the region outside the window. Each Pockels cell had a contrast rejection outside the selected train of 10000:1, which theoretically leads to 0.7% rms modulation in the transmission window (4% peak to valley). These specifications are depicted in Figure 7. The transmission of each Pockels cell was measured to be around 92%, whereas each polarizing beam splitter has a transmission of 95%. The cumulative power transmission of the fast pulse picker was less than 75%.

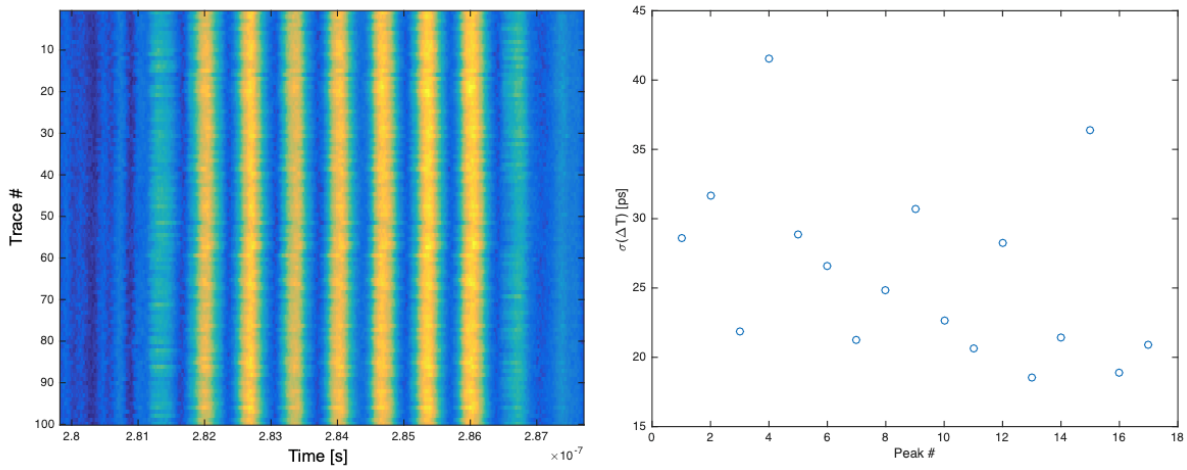

Figure 8: (left) Oscilloscope traces of the 8 ns pulse train. (right) Relative timing jitter between the fast pulse picker trigger and the UV laser pulses, in this case for a 15 ns pulse train.

The performance of the fast pulse picker was tested by measuring the generated pulse train with a 18 GHz bandwidth LeCroy oscilloscope and an ultrafast Si photo-diode (Alphalas UPD-50-UP) with a rise time of less than 50 ps (7 GHz). Even though the individual pulses were not fully resolved, the response of the photo-diode, which is proportional to the individual pulse energy, resembles with high accuracy the temporal transmission profile of the pulse picker.

Firstly, we measured the relative timing jitter between the UV pulse train (locked to the RF reference) and the fast pulse picker trigger signal. This measurement yielded a trigger timing jitter of < 30 ps with respect to the UV pulses, as it can be seen in Figure 8, limited only by the measurement system. In Figure 8, the label 'peak #' denotes the sequential order of the peak of each UV pulse within the train. The temporal position of these peaks was used to estimate the timing jitter with respect to the trigger. In the vertical axis, "$\sigma(\Delta T)$" is the standard deviation of the measured time delay between the trigger signal and each UV pulse peak within the train.

Since the jitter of the trigger of the fast pulse picker system is well below the rise time of the pulse picker window (30 ps vs 400 ps), this trigger can be utilized for measuring the temporal transmission profile of the fast pulse picker itself. This is achieved by running the laser oscillator in open loop mode (free running), and overlapping multiple oscilloscope traces. In this way, the un-locked UV pulse trains 'map' the transmission window of the pulse picker.

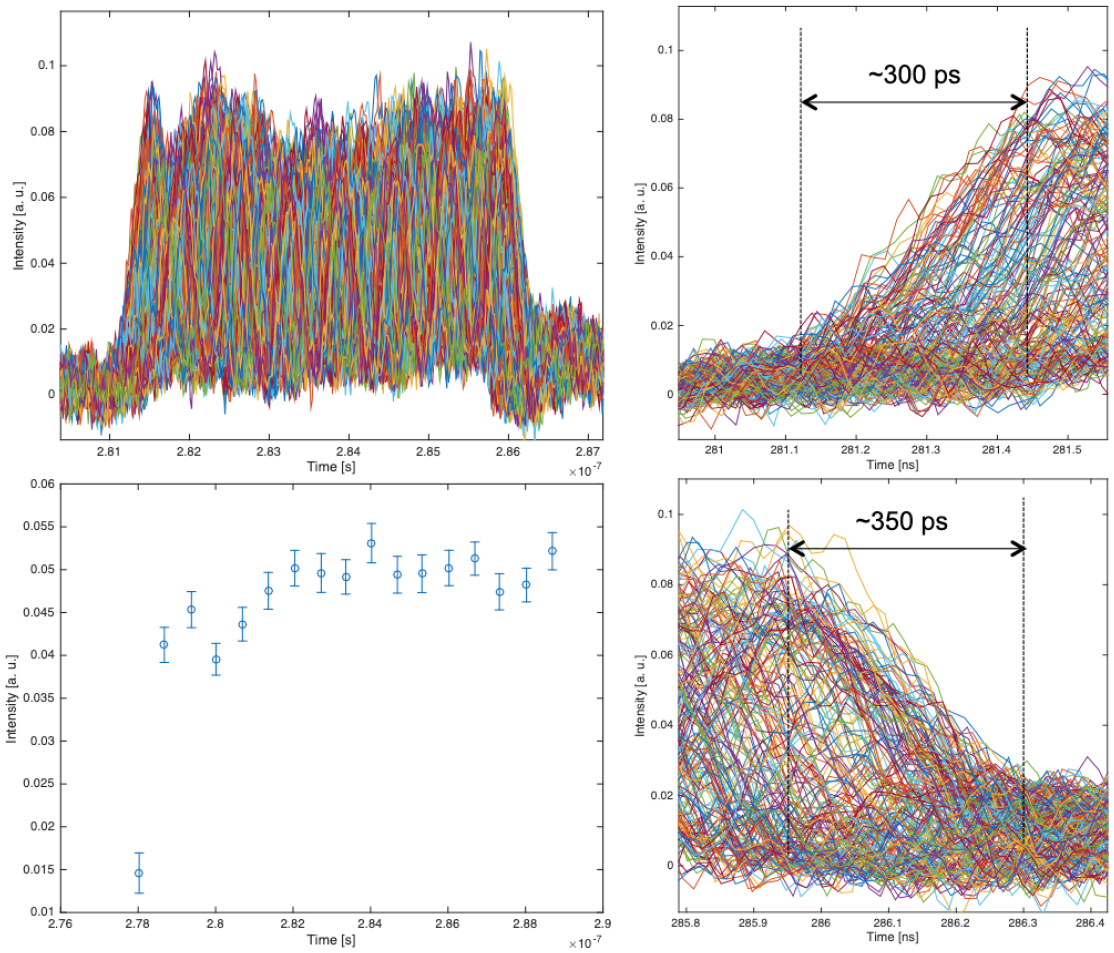

Figure 9: Oscilloscope traces of pulse trains when the oscillator is not locked to the RF reference. Details of the opening and closing slopes for the same temporal window as well as amplitude modulation for a 10 ns pulse train.

Figure 9 shows the measured profile of a 10 ns window (with a close up view of the opening and closing edges). It it is clear that the rising (300 $\pm$ 30 ps) and falling edges (350 $\pm$ 30 ps) of the pulse picker meet the specifications (< 400 ps). However, the relative modulation of the transmission window of the pulse picker is up to $\pm$10%, which is far from the specification of just 0.7%. The residual transmission after the pulse train was not measurable with the current setup, the specification was a residual transmission of <4%, and the results indicate that this requirement was well met.

For temporal windows of a few ns, the envelope of the transmission function is composed by the overlap of both opening and closing temporal profiles of the Pockels cells. As the train duration is elongated, the imprinted transmission fluctuations in amplitude add up quasi-independently. Figure 10 shows the peaks of the pulses in a 80 ns long train pulses (from 100 consecutive traces). Here, the data shows again a modulation of $\pm$10% at the leading edge of the pulse, which decreases with a time constant of 40 ns through the transmission window with a periodicity of approximately 8 ns (125 MHz).

The transmission function profile of the pulse picker arises from the impedance characteristics and bandwidth of the Pockels cell circuit and load. The electrical parameters of the cell were matched to 50 Ω to ensure that the waveform suffers no distortions due to electrical mismatch and cable reflections (large enough reflections can partially re-open the cell after a short time delay). Unfortunately, the internal connections of the Pockels cell typically present a high inductance to truly match to 50 Ω.

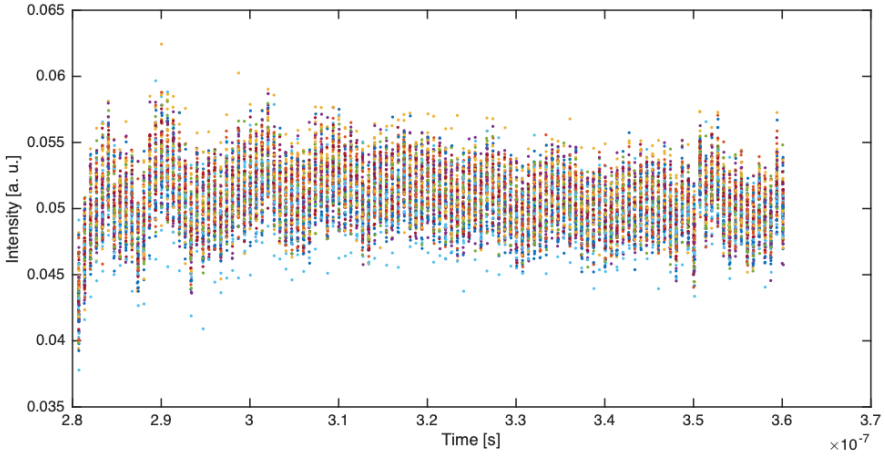

Figure 10: Details of the temporal amplitude modulation of the train for an 80 ns pulse train.

In order to minimize the inductive effects of the Pockels cell, its electrodes were slowly tapered to match the body internal diameter. By using this method, an impedance matched electrical interface loaded the driving circuit, thus minimizing the internal reflections. The dielectric constant of KD*P is very high, and so the propagation of the electrical wave through the optical aperture is in practice relatively "slow". Therefore there is a direct conflict between the requirements of fast switching and a large aperture and it is not possible to obtain ultra fast switching in large aperture cells. This may explain the difference values retrieved for the electrical rise-time of the pulse generator (250 ps) and the optical rise-time of the Pockels cells (400 ps). For our application, the trade off solution was to set the aperture to 5 mm, with a theoretical minimum rise-time of $\sim$ 150 ps if the impedance is perfectly matched across the whole spectrum.

2.2.2 Supercharge mode

As it can be appreciated in Figure 7, a by-pass is used to select either the fast pulse picker system or the so-called "supercharge mode". The switching between the two modes of operation is performed by relocating an intermediate half-wave-plate placed before P1 to the exit of P3 in the fast pulse picker.

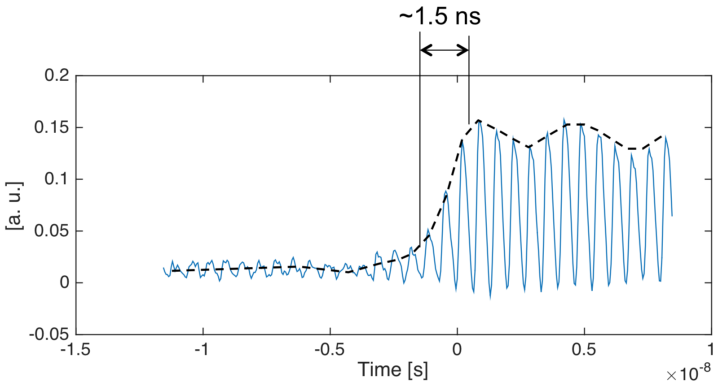

Figure 11: Rise-time of the pulse picker used for the "supercharge" mode.

This mode of operation was constructed in order to enable experiments that require a high radiation

dose on samples. A high dose can be readily achieved by simply stretching the duration of the pulse train further than 120 ns. The pulse picker selected for this purpose was a Leysop BBO-5-40-AR1047, which comprises in the same housing 2 BBO crystals (5x5x20 mm each) and high voltage power supply. A total transmission of around 50% has been measured while switching.

This pulse picker has the capability of producing pulse trains of up to 1 μs. However, its rise time was measured to be around 1.5 ns, as depicted in Figure 11. Therefore, this pulse picker shall not be used for the generation of short pulse trains.

2.3 Main amplifier

The output from the pulse picker system is image relayed onto the main amplifier head by employing a 4f telescope. An isolator was placed before the amplifier to avoid potential back-reflections. The beam is then passed 5 times through the gain media in order to amplify it (5 passes maximizes the extraction efficiency of the amplifier without diffraction effects and a reasonable footprint of $0.5 \times 1.5\,\mathrm{m}$). An schematic of the amplifier is depicted in Figure 12.

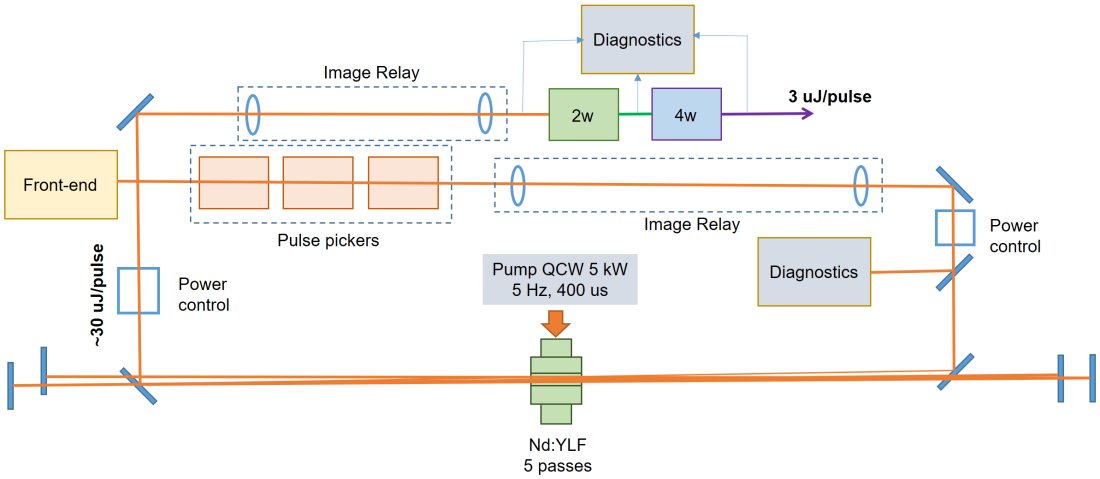

Figure 12: Schematic of the CLEAR laser main amplifier.

The amplifier is comprised of a 44 mm long, 4 mm diameter Nd:YLF rod (with an Nd concentration of 0.8%), housed in a water cooled copper mount. The rod is side pumped by Dilas QCW diodes (400 μs pulses with 5 kW average power during the pulse) at a maximum repetition rate of 5 Hz. Under these conditions, the single pass gain was approximately 8, whereas the gain after 5 passes was of the order of 10^3. After amplification, the pulses had an energy of approximately 30 μJ at 1047 nm. Power control systems were implemented at the input and output of the amplifier.

Since the aperture of the gain medium is relatively small compared to its length, the multi-pass amplifier was designed in a way so each pass impinges the laser medium with the minimum angle of incidence possible. This was achieved by utilizing both azimuthal and tangential planes for each pass through the gain medium.

2.4 Frequency conversion to UV

Frequency conversion is performed with standard non-linear optical crystals. For the second harmonic generation (from 1047 nm to 527 nm), type II conversion in a 10 mm long KTP crystal yields a conversion efficiency of 35%. The spot size in the crystal is approximately 3 mm in diameter ($1/e^2$) with vertical polarization. The output at 527 nm is horizontally polarized with a maximum pulse energy of 15 μJ.

Conversion to the UV is performed in a 12 mm long BBO (type I phase matching), utilizing directly the output from the KTP crystal (similar beam diameter of around 3 mm). The typical efficiency of the process is approximately 30%, bringing the overall efficiency to 10% from IR to UV. A slightly different conversion efficiency was measured for long trains of 100 ns, where the existence of short life-time (ns to ps) color centers in the BBO crystal may play a role.

Table 4: Summary of conversion efficiency from IR to UV.

Parameter	**Single Pulse**	**Long train (100 ns)**
IR to VIS conversion	50%	50%
VIS to UV conversion	Up to 40%	Up to 30%
Typ. IR-UV conversion	Up to 20%	Up to 15%
Typ. UV pulse energy	$\sim 4\mu$J	$\sim 3\mu$J
Max UV energy/bunch at cathode	$\sim 2\mu$J	$\sim 1.5\mu$J

Measuring picosecond duration UV pulses may be challenging due to the lack of transparent non-linear crystals below 200 nm. Commonly, cross-correlation techniques are used in order to convert the UV light to a more convenient to use visible pulse [11]. Since the pulse duration in the IR and the UV are expected to be similar, a cross-correlation measurement would not yield significant information about the pulse shape.

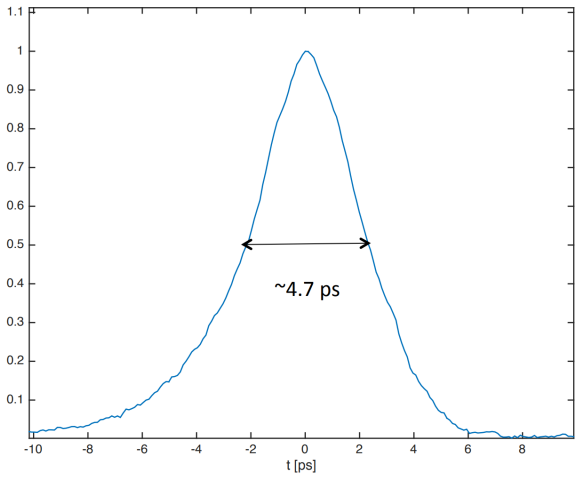

Figure 13: UV pulse temporal profile measured with a high-speed streak camera.

In order to gain a better understanding of the pulse profiles in the UV, which may impact the electron bunch temporal shape, a streak camera was used (with a resolution down to 200 fs when fully optimized). The profile of the output pulses is shown in Figure 13, yielding a pulse duration of approximately 4.7 ps. The pulse shape was slightly asymmetric, with more energy in the trailing edge.

2.5 Double pulse generator

The double pulse generation at CLEAR is based on a common concept around the photo-injector community: pulse stacking. Traditionally, pulse stackers are used in order to achieve high-brilliance and ultra-short FEL pulses by shaping the profile of the UV pulses. The so-called pulse stacking technique involves the production of replicas of a single UV laser pulse. The temporal superposition of these gives

the picosecond a flat-top amplitude when the various pulses partially overlap in time, reducing space charge effects. As the delay between replicas is increased beyond the pulse duration, multiple electron bunches can be generated within the same RF cycle.

For splitting and recombining the UV pulses, a modified Mach-Zender interferometer was used (see Figure 14). The laser pulse was first divided into two by a polarizing beam splitter (PBS1) so that the P-polarized beam goes straight and the S-polarized beam is reflected sideways. The ratio of power between each beam is controlled by the half-waveplate HWP1. Each of the beams (P and S) hit the set of mirrors and then they are recombined by another polarizing beam splitter cube (PBS2). One set of mirrors was positioned on a movable platform so that the delay between the two beams can be adjusted. A second half-wave plate (HWP2) provided adjustment of the intensity of the main beam.

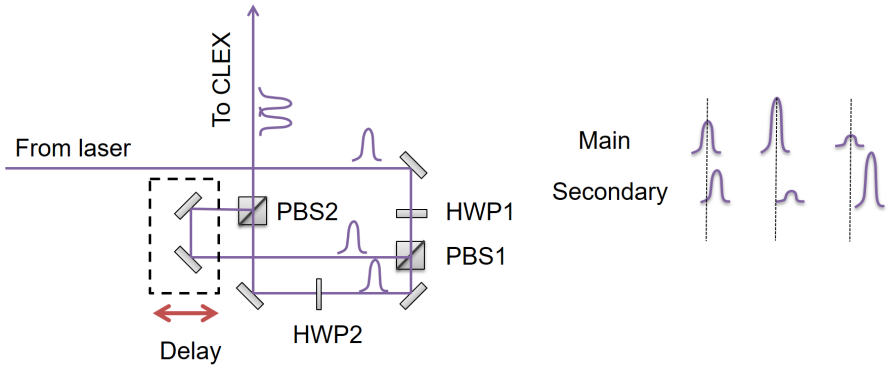

Figure 14: Double pulse generation setup

Both wave-plates and delay stage are motorized for remote control, while PBS2 has 2-axis motorization (tip-tilt) in order to gain independent alignment of the two beams on the cathode. The delay stage provides a temporal resolution of 17 fs, with a delay range of up to 1 ns. This wide range opens the possibility of even doubling the repetition rate of the laser to 3 GHz, if a delay of 333 ps is set. The tip-tilt of PBS2 is performed using a stepper motor actuated high precision mount, with a resolution of 0.0016 degrees.

In terms of contrast, the PBS (from Spectral Products, model PCBS-MF-262-100-F) have a contrast of 100:1 between transmission of P-polarized light and reflection of S-polarized light. This means that, in the best case scenario, a leak of 1% from one of the arms will be always leaked through the double pulse generation setup onto the cathode. For avoiding this scenario, remote controlled motorized beam stoppers have been installed in each arm. The double pulse setup also serves as power control for the UV beam, by tuning either HWP1 or HWP2.

It is important to note that the output pulses from the stacker have P and S polarization. In order to effectively use the diagnostics existing in the CLEX experimental area (which are polarization sensitive), the output of the stacker was rotated by 45 degrees by using an additional half wave-plate at the exit of the double pulse setup.

2.6 Transfer line to the CLEX experimental area

The distance from the laser room to the photo-cathode is about 70 m (see Figure 15). Optical relay was needed in order to minimize the consequences of disturbances of the beam alignment along the path (tilt of mirrors, displacement of components by vibration, thermal expansions, as well as turbulence). The initial design for the laser diameter on the photo-cathode was 4 mm $\pm$ 10% with position instability of less than 10% of the diameter (i.e 0.4 mm).

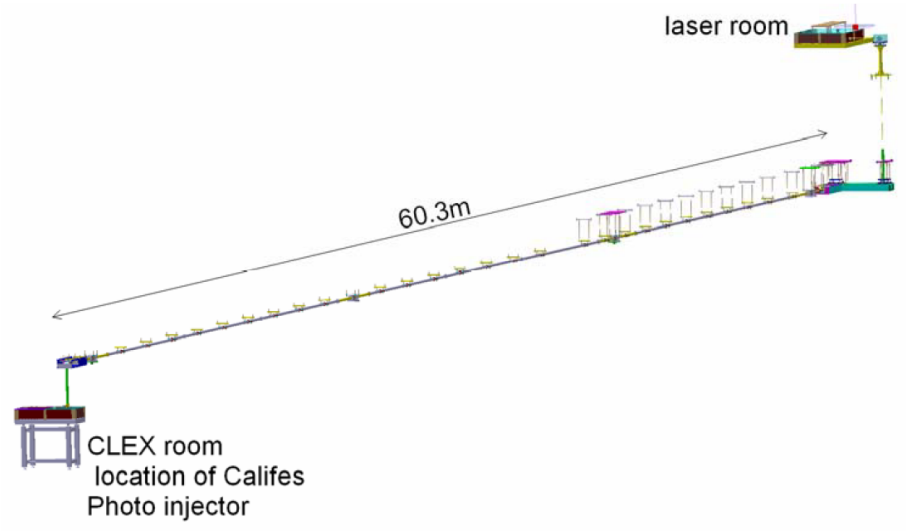

Figure 15: View of the beam transport between laser room and CLEX experimental area.

Two 4f telescopes were used for optical relay; the first telescope transports over 30 m (with two 7.5 m focal length lenses) and the second transports over 40 m (with two 7.5 m focal length lenses). The magnification of each telescope relay is 1. A major modification of the imaging condition was carried out around 2012, when a 2 m long focal length lens was introduced in the CLEX area to loosely focus the UV beam into a 1 mm diameter spot onto the cathode. Analogously, a 3 lens afocal zoom telescope was removed in the laser room (located after harmonic conversion stages). The modifications were done to accommodate for optical elements needed for the construction of the CLEAR main amplifier. Those modifications affected the beam stability, which decreased to around 30% of the beam diameter due to the lack of strict relay imaging condition between laser media and photo-cathode surface.

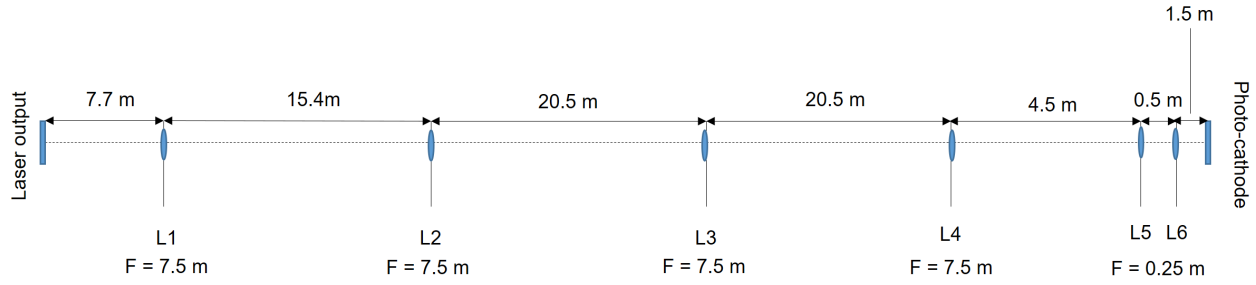

Figure 16: Schematic of the optical transport from the laser room to the photo-injector optical table.

In order to improve the beam stability while maintaining a relatively small beam diameter, a compact 4f de-magnifying relay telescope has been introduced in the CLEX area. With this modification, the layout of the transfer line between laser room and photo-cathode is depicted in Figure 16. ABCD transfer matrices were used to calculate the position of the image plane of the photo-cathode in the laser room. The distance was calculated from L1 towards the laser room, and was found to be around 12 m in normal conditions (4.3 m before the laser lab output).

2.7 Variable spot size on the photo-cathode

Transverse adjustment of the UV laser beam is done in order to optimize the laser fluence in the photo-cathode for each particular CLEAR experiment. Variation of the spot size may be required, for example, to minimize electron beam emittance or to obtain a higher charge per bunch (by maximizing the charge yield of the RF gun). Several approaches exist to achieve this, for instance image relaying a variable diameter aperture onto the photo-cathode has been done successfully at AWAKE. At CLEAR, in order to add flexibility of spot size while delivering the full pulse energy to the RF gun, a variable mismatched telescope has been introduced.

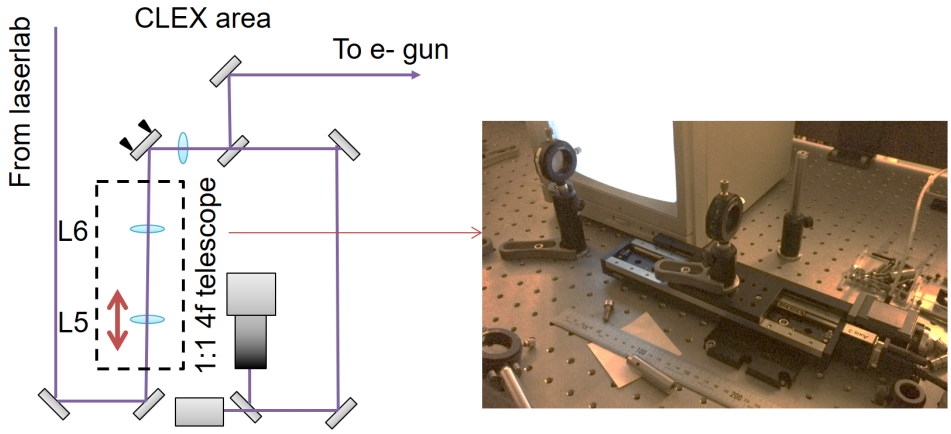

Figure 17: Setup for the variable spot size on the photo-cathode.

After the introduction of the compact relay image telescope comprised of L5 and L6, a motorized translation stage was installed for L5 with the purpose of providing users with a variable laser spot size on the photo-cathode. Obviously, for a large change in position of L5, the imaging condition into the photo-cathode will be lost. This could be further optimized in the future by employing an afocal zoom telescope instead, although here, for simplicity, a 2 lens telescope was enough for producing the range of spot sizes necessary for experiments as shown in Figure 17.

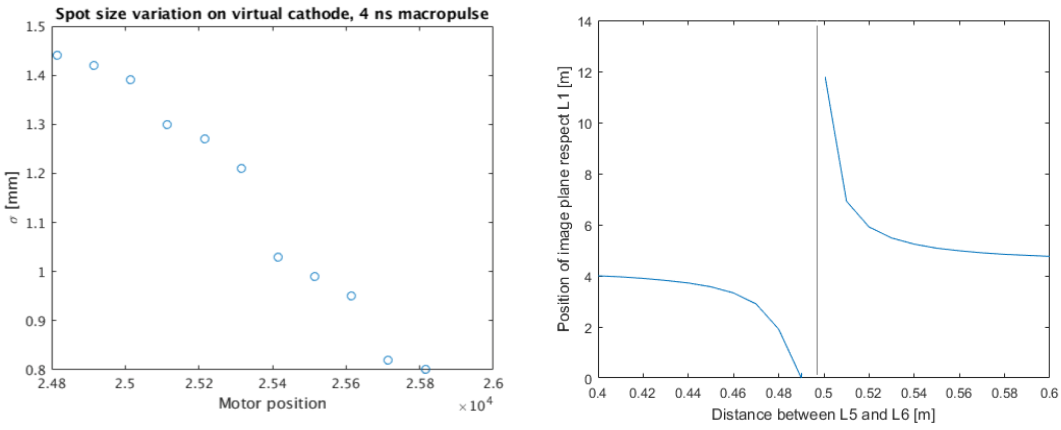

Figure 18: (left) Spot size on photo-cathode as a function of L5 motor position. (right) Simulation of the image plane position with respect to L1 while varying the position of L5.

Figure 18 shows an example of spot size impinging on the photo-cathode while varying the pos-

ition of the lens L5. Only a portion of the translation stage is shown since positioning the lens further produces a spot size small enough to potentially damage the surface of the photo-cathode. The spot size was measured directly from the profiles measured at the virtual cathode imaging system.

Changing the position of the lens L5 has also consequences in terms of the relay image condition between the laser output and the photo-cathode. Employing ABCD transfer matrices simulations, it can be seen that shortening or enlarging the distance between L5 and L6 by 10 cm, changes the image plane position in the laser room by a few meters. This is shown in the simulation results depicted in Figure 18 (right). The main consequence of this effect is a larger spatial jitter when the beam size is increased. For a distance of 0.496 m, the image plane is in the infinite (discontinuity shown in the plot).

3 Conclusions and future outlook

The CLEAR facility delivered its first beam in mid-August 2017, and experiments were resumed in September of the same year. A campaign of measurements is ongoing with the aim of exploit the full capabilities of the present installation.

Currently, studies for injector optimization are ongoing with the aim to allow for reaching sub-ps bunch lengths. CLIC related studies have been resumed, as well as irradiation campaigns in collaboration with the European Space Agency (ESA) and the TRAD Tests Radiations company. First beams were also delivered to the novel plasma-lens experiment which is now fully installed and ready for measurements. The development for a new Electro Optical BPM for HL-LHC and impedance measurements of a wire scanner for the Super Proton Synchrotron (SPS).

Further improvements and developments are foreseen in the CLEAR photo-injector laser installation in order to expand and enhance the current capabilities. These include: improvement of shot-to-shot stability of UV pulse in terms of energy and pointing, optimization of variable spot size setup, new control systems architecture and diagnostics, and implementation of a second femtosecond electron gun for future pump-probe experiments.

Bibliography

[1] D. Gamba, R. Corsini, S. Curt, S. Doebert, W. Farabolini, G. Mcmonagle, P.K. Skowronski, F. Tecker, S. Zeeshan, E. Adli, C.A. LindstrÃÿm, A. Ross, L.M. Wroe, The CLEAR user facility at CERN, Nuclear Instruments and Methods in Physics Research Section A: Accelerators, Spectrometers, Detectors and Associated Equipment, Volume 909, Pages 480-483, (2018).
http://cds.cern.ch/record/2665487?ln=en.

[2] CEA document NT DPC / SCP 08-278-A.

[3] Mosnier A., et al. The probe beam linac in CTF3 Proceedings of the 10th European Particle accelerator Conference, EPAC2006, vol. C060626 (2006), pp. 679-681 Edinburgh, UK.
https://accelconf.web.cern.ch/AccelConf/e06/PAPERS/MOPLS059.PDF

[4] W. Farabolini, CTF3 probe beam LINAC commissioning and operations, in: Proceedings, 25th International Linear Accelerator Conference, LINAC2010: Tsukuba, Japan, September 12-17, 2010, 2011, p. MOP001.
http://accelconf.web.cern.ch/AccelConf/LINAC2010/papers/mop001.pdf

[5] E. Chevallay, Experimental Results at the CERN Photoemission Laboratory with Co-deposition Photocathodes in the Frame of the CLIC Studies. Tech. Rep. EDMS n. 1215630. CTF3-Note-104, CERN, Geneva (2013).
http://clic-study.web.cern.ch/sites/clic-study.web.cern.ch/themes/cliccern/pdfs/notes/CTF3Note104.pdf

[6] J. L. Navarro Quirante, R. Corsini, A. Grudiev, T. Lefevre, S. Mazzoni, R. Pan, F. Tecker, W. Farabolini, F. Peauger, D. Gamba et al. CALIFES: A Multi-Purpose Electron Beam for Accelerator Technology Tests. 27th International Linear Accelerator Conference (LINAC14), p.MOPP030 (2014).
http://accelconf.web.cern.ch/AccelConf/linac2014/papers/mopp030.pdf

[7] M. Petrarca, V. Fedosseev, N. Lebas, and G. Cheymol. CTF3 photo-injector laser system: Conversion to UV. CARE-Report-2008-019-PHIN (2008).
http://irfu.cea.fr/Phocea/file.php?class=std&&file=Doc/Care/care-report-08-019.pdf

[8] M. Petrarca, K. Elsener, V. Fedosseev, N. Lebas. CTF3 photoinjector: RF synchronisation of the laser system. CARE-Report-2008-030-PHIN (2008).
http://irfu.cea.fr/Phocea/file.php?class=std&&file=Doc/Care/care-report-08-030.pdf

[9] R. Losito, H.-H. Braun, N. Champault, E. Chevallay, V. Fedosseev, A. Kumar, A. Masi, G. Suberlucq, M. Divall, G. Hirst, G. Kurdi, W. Martin, I. Musgrave, I. Ross, E. Springate, G. Bienvenu, B. Mercier, C. Prevost, R. Roux. The PHIN photoinjector for the CTF3 Drive beam. CERN-AB-2006-074 ; CLIC-Note-684 ; CTF3-Note-078 ; CARE-Conf-06-019-PHIN ; CARE-Conf-2006-019-PHIN (2006).
http://cds.cern.ch/record/972359

[10] W. Kester, Converting oscillator phase noise to time jitter, Analog Devices, Inc., Tutorial MT-008.
https://www.analog.com/media/en/training-seminars/tutorials/MT-008.pdf

[11] E. Granados, A. Fuerbach, D.W. Coutts, and D.J. Spence. Asynchronous cross-correlation for weak ultrafast deep ultraviolet laser pulses. Applied Physics B 97(4):759-763 (2009).
https://link.springer.com/article/10.1007/s00340-009-3634-5